PCCP

ARTICLE

Two photon spectroscopy and microscopy of the fluorescent flavoprotein, iLOV

Received 00th January 20xx,
Accepted 00th January 20xx

DOI: 10.1039/x0xx00000x

www.rsc.org/

Rachael J. Homans,[†a,b] Raja U. Khan, [†a,b] Michael B. Andrews,[a] Annemette E. Kjeldsen,[c] Louise S. Natrajan,[a] Steven Marsden,[d] Edward A. McKenzie,[b] John M. Christie[c] and Alex R. Jones*[a,b,e]

LOV-domains are ubiquitous photosensory proteins that are commonly re-engineered to serve as powerful and versatile fluorescent proteins and optogenetic tools. The photoactive, flavin chromophore, however, is excited using short wavelengths of light in the blue and UV, which have limited penetration into biological samples and can cause photodamage. Here, we have used non-linear spectroscopy and microscopy of the fluorescent protein, iLOV, to reveal that functional variants of LOV can be activated to great effect by two non-resonant photons of lower energy, near infrared light, not only in solution but also in biological samples. The two photon cross section of iLOV has a significantly blue-shifted $S_0 \rightarrow S_1$ transition compared with the one photon absorption spectrum, suggesting preferential population of excited vibronic states. It is highly likely, therefore, that the two photon absorption wavelength of engineered, LOV-based tools is tuneable. We also demonstrate for the first time two photon imaging using iLOV in human epithelial kidney cells.. Consequently, two photon absorption by engineered, flavin-based bio-molecular tools can enable non-invasive activation with high depth resolution and the potential for not only improved image clarity but also enhanced spatiotemporal control for optogenetic applications.

Introduction

LOV (light, oxygen, or voltage) domains are blue light photoreceptor proteins that contain a non-covalently bound flavin mononucleotide (FMN) as photoactive chromophore (Figure 1).[1, 2] In wild-type LOV domains, photoexcitation of FMN leads to intersystem crossing,[3, 4] and from the protonated triplet state a covalent adduct is formed between the C4a of FMN and a neighbouring cysteine residue.[5] These photophysical and photochemical events suppress the fluorescence of the FMN, and instead channel much of the absorbed light energy towards adduct formation and subsequent changes to protein structure.[6] LOV serves as a ubiquitous photosensory domain the light-triggered structural changes of which are known to modulate the activity of a remarkably diverse range of effector domains.[7, 8] The sensor / effector combinations often adopt complex, multidomain architectures allowing LOV domains to effect a wide variety of functions in response to light. These include the ability of plants to enhance the efficiency of photosynthesis through the action of LOV-based blue-light receptor kinases known as the phototropins.[1] In addition, LOV-containing photoreceptors facilitate circadian regulation in fungi *e.g.*,[9] and mediate a wide variety of functions in bacteria[2] ranging from cell adhesion to stress responses.

Their modularity and functional versatility mean that engineered LOV domains have demonstrated significant utility as molecular tools for both the control and imaging of biological systems. They are one of the most commonly adapted systems for optogenetic applications.[10] Here, the genes that encode engineered photoreceptor proteins are expressed in target cells to enable the optical control of a biological function of interest. LOV domains have also been engineered as fluorescent proteins (FPs) that, after excitation of the FMN with blue light, emit in the green.[13, 14] For example, mutations to the monomeric LOV2

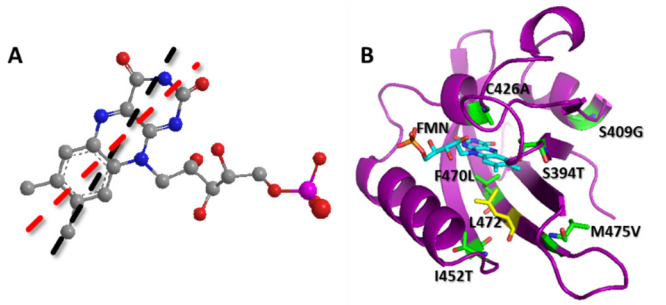

Figure 1A. Flavin mononucleotide (FMN), with the approximate $S_0 \rightarrow S_1$ and $S_0 \rightarrow S_2$ transition dipoles for the one photon absorption of the isoalloxazine chromophore indicated with black and red dashed lines, respectively.[11] Grey – carbon; blue – nitrogen; red – oxygen; pink – phosphorous. **B.** X-ray crystal structure of iLOV (PDB: 4EES),[12] with bound FMN (blue). iLOV is an engineered, fluorescent variant of the monomeric LOV2 domain from *Arabidopsis thaliana* phototropin 2; the mutated residues (green) are labelled. Although not mutated, L472 (yellow) becomes re-orientated in iLOV, which is thought to contribute to its improved fluorescence quantum yield.[12]

[a.] *School of Chemistry and Photon Science Institute, The University of Manchester, Oxford Road, Manchester, M13 9PL, UK.*
[b.] *Manchester Institute of Biotechnology, The University of Manchester, 131 Princess Street, Manchester, M1 7DN, UK.*
[c.] *Institute of Molecular, Cell and Systems Biology, College of Medical, Veterinary and Life Sciences, Bower Building, University of Glasgow, Glasgow, G12 8QQ, UK*
[d.] *School of Biological Sciences, The University of Manchester, Oxford Road, Manchester, M13 9PL, UK*
[e.] *Current Address: National Physical Laboratory, Hampton Road, Teddington, Middlesex, TW11 0LW, UK*
† RJH and RUK contributed equally to this work. *alex.jones@npl.co.uk
Electronic Supplementary Information (ESI) available. See DOI: 10.1039/x0xx00000x

domain from *Arabidopsis thaliana* phototropin 2 (Figure 1B) – including the adduct-forming cysteine to alanine – have produced a FP designated iLOV ("improved LOV").[15] Unlike traditional green fluorescent protein (GFP), the green-emitting iLOV and similar LOV-based FPs derived from plants[12, 16] and microorganisms[17-21] do not require an aerobic environment for fluorescence, are significantly less sensitive to pH and some have even been reported to recover after photobleaching.[*e.g.*, 15] Their relatively small size (iLOV ~12 kDa) and monomeric structure mean that plant-based LOV FPs are superior fluorescent reporters to GFP (~27 kDa) in contexts where the size of the biomolecular assembly influences function; *e.g.*, plant[15] and animal[22] RNA viral infection and movement. Finally, the rapid onset of fluorescence after expression of LOV-based FPs (within a few minutes) compared to GFP (tens of minutes)[18] means they have greater utility as real time *in vivo* reporters.[23]

Despite the potential versatility of LOV-based biomolecular tools, flavin-based photoreceptors are activated using short-wavelength (UV-blue) light.[24] This represents a significant limitation; such high energy photons can interact strongly with biological samples, which severely limits tissue penetration and can cause collateral photodamage. Moreover, blue light photoreceptors are widespread in nature,[24] and therefore the use of unfocussed blue light to activate an optogentic tool or FP runs the risk of also activating endogenous photoreceptors and therefore stimulating off-target responses. The $S_0 \rightarrow S_1$ and $S_0 \rightarrow S_2$ electronic transitions of the isoalloxazine chromophore of FMN (Figure 1A), however, are also known to be possible using two non-resonant photons of near infrared (NIR) light.[25-27] Indeed, two photon (2P) excitation has been demonstrated for the LOV-derived protein, miniSOG, which generates reactive oxygen species in response to light.[27] NIR overcomes many of the problems associated with shorter wavelength light, and 2P microscopy is now a common tool for non-invasive bioimaging using fluorescent labels[28] and label free second harmonic generation,[29] especially when relatively deep tissue penetration is desired. Because 2P excitation requires significant flux densities, it often only occurs at the sub-femtolitre focal point of a laser beam passed through a high numerical aperture (NA) objective lens.[30] It therefore enables superior three-dimensional (3D) spatial resolution for both imaging[30] and optogenetic activation.[31]

Results and Discussion

We have therefore investigated whether the FMN bound to a LOV domain (iLOV, Figure 1B) is amenable to 2P excitation *in vitro* and to 2P imaging in human epithelial kidney (HEK) cells, using wavelengths in the NIR. The one photon (1P) absorption and emission spectra of FMN bound to iLOV are shown in Figure 2A. The $S_0 \rightarrow S_1$ transition peaks in the blue (λ_{max} ~ 448 nm) and shows the distinctive vibronic structure[32] often observed for flavins in a protein environment. The emission peak for iLOV is blue-shifted by around 35 nm compared to that of free FMN (λ_{max} ~ 496 nm), and again vibrational structure is evident; both features are typical for LOV-based FPs.[*e.g.*,33] We determined the fluorescence quantum yield, Φ_F, following 1P excitation of iLOV

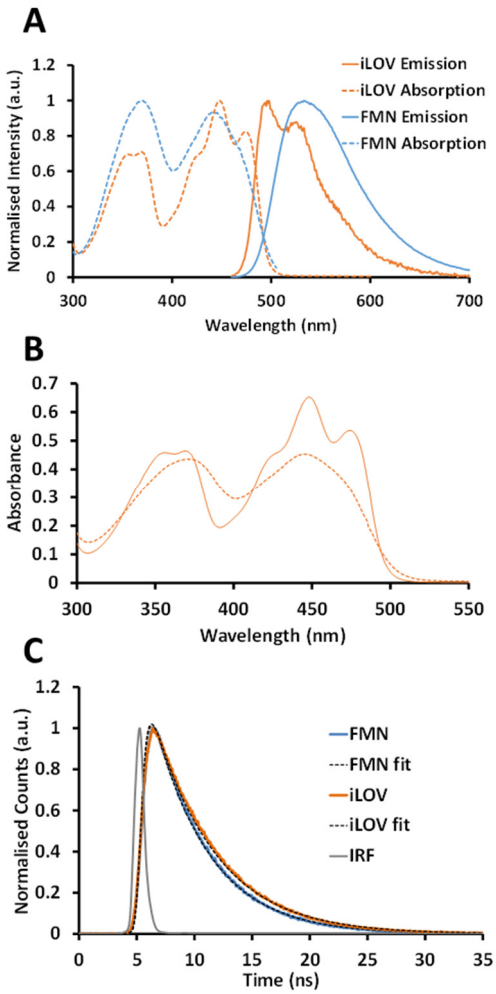

Figure 2A. Absorption (dashed) and emission (solid) spectra of FMN (blue) and iLOV (orange). **B.** Absorption spectra of iLOV (solid) and the same concentration of FMN (dashed) liberated from the protein, revealing an enhanced molar extinction coefficient for FMN bound to iLOV around the $S_0 \rightarrow S_1$ transition. **C.** Fluorescence lifetime data (solid) and single exponential fits (dashed) for FMN (blue) and iLOV (orange) after photoexcitation at 474 nm. IRF (grey): instrument response function.

to be ~ 0.30 (Figure S1, Supporting Information). This is lower than initially reported for iLOV (Φ_F ~ 0.44),[15] which was calculated based on the assumption that the molar extinction coefficients, ε, for FMN and iLOV are the same, and is in line with more recent estimates (0.34[18] and 0.33[34]). If FMN is released from iLOV, however, it is clear that, like with many other LOV-based FPs,[33] the ε of FMN around the $S_0 \rightarrow S_1$ transition is significantly enhanced in iLOV (Figure 2B).[34] Whilst the ε at ~ 450 nm of FMN in aqueous solution is 12.2 mM^{-1} cm^{-1},[33] based on the spectra in Figure 2A this increases substantially to ~ 17.6 mM^{-1} cm^{-1} when bound to iLOV. The fluorescence lifetime, τ, of iLOV (Figure 2C, τ = 5.27 ± 0.01 ns) is longer than that of free FMN (τ = 4.38 ± 0.30 ns). Such extended lifetimes are also significantly longer than those of GFP derivatives, most of which are < 4 ns.[35] It has therefore been proposed[33] that many LOV-based FPs are more suitable than GFPs for Förster resonance energy transfer (FRET) imaging[36] that is combined with fluorescence lifetime imaging microscopy (*i.e.*, FRET-FLIM).[37]

To initially investigate the potential for non-linear activation of LOV-based optical tools, 2P fluorescence spectroscopy[38, 39] was conducted with iLOV. Femtosecond pulses from a Mai Tai oscillator were focussed onto the sample using a 40×, 0.6 NA microscope objective with an extra-long working distance (ELWD), and the fluorescence intensity was measured as a function of laser power and excitation wavelength (see Experimental Section). Figure 3A shows example fluorescence data as a function of laser power after the excitation of iLOV at 860 nm, and Figure 3B illustrates the non-linear dependence of the integrated emission intensity on laser power. Equivalent data for FMN in aqueous solution can be found in the Supporting Information (Figures S2A&B). The plot in Figure 3C of $\log_{10}$(integrated intensity) *vs.* $\log_{10}$(laser power) confirms that the $S_0 \rightarrow S_1$ transition preceding the measured fluorescence from iLOV is owing to 2P excitation by the 860 nm NIR light, with a gradient of ~ 1.96. Although this gradient for iLOV and for free FMN (Figure S2C) are almost exactly equal to 2, there is a significant sub-quadratic dependence following 2P excitation of the $S_0 \rightarrow S_2$ transitions (*e.g.*, 730 nm, Figure S3A, Supporting Information). Such a dependence can be attributed to a number of factors, but is most likely owing to stimulated emission by the focussed beam at higher laser powers[40] (otherwise known as 'light quenching').[41] Whilst the direction of spontaneous emission is random, photons from stimulated emission are always directed along the incident laser path and therefore never reach the detector, hence a sub-quadratic dependence. This effect of stimulated emission was overcome by conducting the laser power dependence over a range below ~ 10 mW (Figure S3B, Supporting Information).

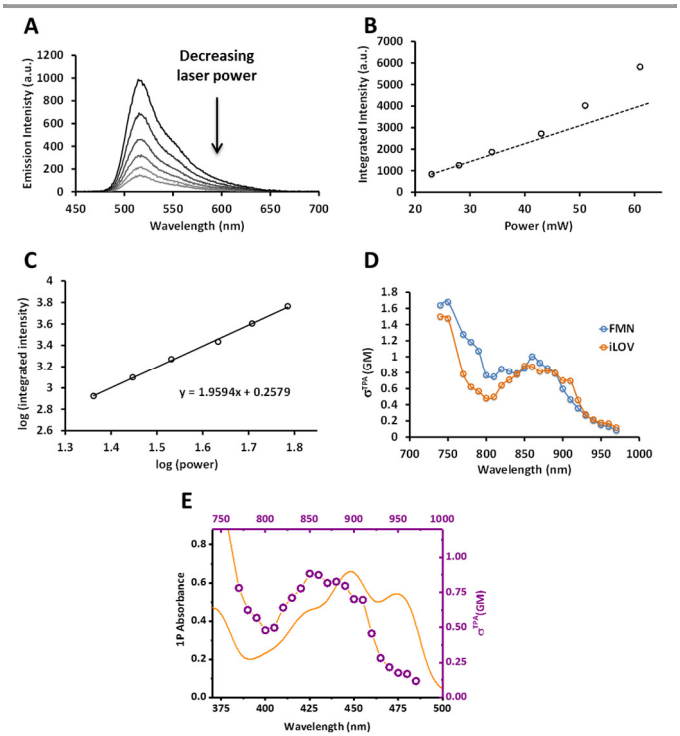

Figure 3. The 2P fluorescence spectrum (**A**) and integrated emission intensity (**B**) of iLOV as a function of excitation laser (860 nm) power. The dashed line in **B** helps to illustrate the non-linear dependence of emission intensity on laser power. **C.** $\log_{10}$(integrated emission intensity) as a function of $\log_{10}$(laser power), with corresponding linear fit of gradient ~ 1.96. **D.** 2P absorption cross section (σ^{TPA}) spectrum of FMN in aqueous solution (blue) and bound to iLOV (orange). **E.** 1P (orange line) and 2P (purple circles, orange line) absorption spectra of iLOV illustrating the ~ 40 nm blue shift of the 2P $S_0 \rightarrow S_1$ transition peak relative to the 1P peak.

Laser power-dependencies were measured for iLOV and FMN as a function of 2P excitation wavelength (730 – 970 nm). The 2P absorption cross section (σ^{TPA}) spectra (Figure 3D) were then calculated[42] with reference to concurrent and equivalent measurements with a fluorescent standard that has a known and appropriate σ^{TPA} spectrum (fluorescein,[43] Figure S4, Supporting Information). Refer to the Experimental Section for full details. Where there is overlap, the σ^{TPA} spectrum of FMN in solution is almost identical to that published recently for the wavelength range 630 – 900 nm.[27] The σ^{TPA} spectrum of FMN bound to iLOV is qualitatively very similar; both spectra have peaks at around 750 and 860 nm, with the short wavelength signal having a significantly higher intensity. The relative peak intensities in the σ^{TPA} spectrum of iLOV are the opposite of those observed for the 1P absorption spectrum (Figure 2A), which, for a similar LOV-based protein, has been attributed to a larger contribution from the dipolar term to the 2P transition matrix element.[27]

Whereas the 750 nm peak in the 2P spectrum appears to be at roughly twice the wavelength of the equivalent transition in the 1P spectrum, the 860 nm peak is blue-shifted by at least 40 nm (Figure 3E). This is perhaps surprising for the isoalloxazine chromophore in FMN (Figure 1A), which does not have an inversion centre and is thus expected to have a 2P spectrum that corresponds to the 1P spectrum but at twice the wavelength.[38] The $S_0 \rightarrow S_1$ transition peak might therefore be expected at around 900 nm (Figure 3E). A similar blue-shift in the 2P spectrum of the GFP variant, enhanced GFP, was proposed to be owing to the population of a 'hidden' excited state with a significantly higher transition probability for 2P than for 1P absorption.[44] An alternative hypothesis was offered to explain the blue-shifted 2P spectra of orange and red FPs, where it was argued that the signal intensity compared to the 1P spectrum in each case is redistributed towards a vibronic peak at shorter wavelengths.[45] This interpretation is supported by computational simulations of 2P and 1P spectra of GFP,[46] which suggest non-Condon effects that result in preferential population of excited vibrational levels of the S_1 state owing to a change in the transition dipole moment from 1P to 2P absorption. Indeed, the 860 nm peak in the iLOV 2P spectrum does coincide with the vibrational shoulder of the $S_0 \rightarrow S_1$ transition in the 1P spectrum (*i.e.*, at ~ 430 nm) and there appears to be a shoulder at around 900 nm in the 2P spectrum (Figure 3E). These observations are certainly consistent with a redistribution of peak intensities between vibronic states, but will need to be corroborated with computational studies into the 2P absorption properties of FMN similar to those conducted for miniSOG.[27] Because FMN and iLOV both have 2P spectral peaks at around 860 nm (Figure 3D) the physical origin of this blue-shift is not owing to binding of FMN to the protein *per se* and must therefore be an intrinsic property of the chromophore electronic structure. That said, different extents of blue-shift have been reported for the same chromophore in different red

FPs,[47] and the 2P cross section of a FP chromophore can also vary substantially in different electrostatic environments.[48, 49] It is therefore likely that the 2P absorption properties of FMN can also be tuned by the protein environment to some extent and that therefore LOV-based FPs and optogenetic tools can be tailored for different 2P activation wavelengths.

Figure 4 compares 1P and 2P fluorescence microscopy images of HEK cells expressing iLOV that were acquired using a Leica SP8 Upright Multi-Photon Microscope and a 40×, 1.10 NA water-immersion objective lens. Refer to the Experimental Section for full details. Improved image clarity is apparent after 2P excitation using both 860 nm (Figure 4B) and 900 nm (Figure 4D) when compared to the equivalent 1P (488 nm, Figures 4A and 4C, respectively) image of the same cell or cells. This is true whether the 2P image was acquired first (as in Figures 4A&B) or the 1P image was acquired first (as in Figures 4C&D), and is therefore not an artefact of the bleaching of iLOV fluorescence following the acquisition of the 2P image. To probe this observation further, a comparison was made of the fluorescence intensity profiles across a line of pixels on equivalent 1P and 2P images (Figure S5). Any loss of clarity in the 1P image is likely to be a result of excess out-of-focus light (see discussion below), which would broaden the features on the intensity profile. Consistent with this, the profile from the 2P image does contain slightly sharper, narrower features than that from the 1P image. It is also likely, however, that a significant contributing factor to any apparent gain in clarity will be that the 2P images are marginally brighter (Figure S5B) owing to the necessarily higher laser power used in the 2P experiments.

Aside from the potential for a marginal gain in image clarity, the benefits of 2P microscopyare at least twofold. First, 2P microscopy using iLOV will provide images with high depth resolution. If there is less out-of-focus light polluting the 2P image it is almost certainly owing to the fact iLOV is only excited by 2P in a small very volume at the focal depth of the microscope objective.[30] 1P excitation, by contrast, occurs throughout the sample depth and thus emission from parts of the sample above and below the chosen focal plane can also be detected, thus muddying the image contrast and limiting depth resolution. Second, such fine depth resolution suggests that 2P activation of LOV-based optogenetic tools will enable high-precision, 4D spatiotemporal control. Optogenetics using 1P activation and pulsed light sources has proven such a powerful tool in areas such as neuroscience[51] because it allows targeted control in both time and space. Because 2P excitation occurs in such a small volume, the spatial accuracy will not only improve in the X-Y focal plane, but also in the Z-direction (*i.e.*, 3D spatial control). Indeed, 2P activation of channelrhodopsin variants has previously been exploited to control the activity of neurons in culture, slices and *in vivo* at the level of single cells.[31] Furthermore, the use of femtosecond lasers – which provide the necessary photon flux for 2P excitation – in combination with new camera technology that enables frame rates of up to 100 gigaframes per second, has the potential to push the accuracy in the temporal dimension into the ultrafast regime.[52]

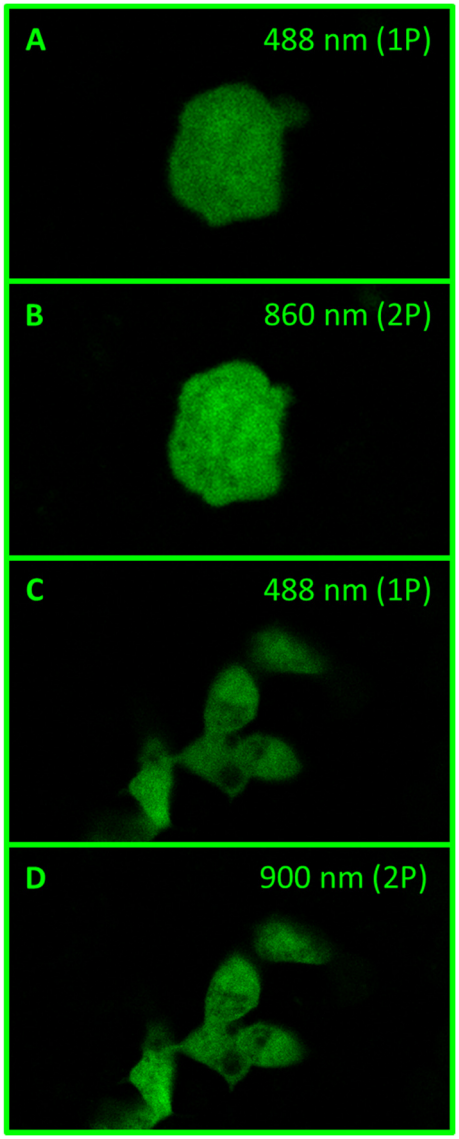

Figure 4. Comparison of: the 1P (**A**, 488 nm) and 2P (**B**, 860 nm) images of a single HEK293 cell expressing iLOV; the 1P (**C**, 488 nm) and 2P (**D**, 900 nm) images of a group of HEK cells expressing iLOV. A gain in image clarity from 1P to 2P excitation of iLOV is apparent in each case. Such a gain is not observed when comparing 1P and 2P excitation of the $S_0 \rightarrow S_2$ transition (Figure S6).

Conclusions

In summary, we have reported the first detailed investigation of the 2P activation of an engineered LOV variant in both solution and in human cells. In doing so, we show that the extinction coefficient for the $S_0 \rightarrow S_1$ transition peak (~450 nm) of the iLOV 1P absorption spectrum is significantly enhanced (~17.6 mM^{-1} cm^{-1}) when compared to FMN free in aqueous solution (~12.2 mM^{-1} cm^{-1}). We have therefore been able to calculate a more accurate fluorescence quantum yield for iLOV (~0.3) than those reported previously.[15, 18] Both this and the fluorescence lifetime (> 5 ns) are enhanced over free FMN, which makes iLOV a suitable energy donor in FRET-FLIM experiments.[33] The 2P absorption spectrum of FMN and iLOV are very similar. The peak of each 2P $S_0 \rightarrow S_1$ transition is at ~ 860 nm and is therefore

blue-shifted by at least 40 nm from what is expected from the 1P spectrum (~ 900 nm). This shift is most likely owing to preferential population of an excited vibronic state,[49] which is in principle sensitive to the electrostatic environment of the chromophore.[47] The 2P activation wavelength of LOV-based tools is therefore likely to be tuneable. We reveal for the first time that 2P imaging using iLOV and NIR in HEK cells, with an apparent improvement in image clarity compared to the corresponding 1P image using an excitation wavelength of 488 nm. iLOV is only excited by 2P at the small focal volume of the laser, which means the image in the X-Y plane is not obscured by out-of-focus light from different sample depths and by implication that the Z (depth) resolution is high. In combination with short laser pulses, the high spatial resolution afforded by the 2P activation of LOV-based tools will facilitate enhanced 4D (spatiotemporal) resolution for both imaging and optogenetic control.

Experimental

Expression and purification of recombinant iLOV

iLOV was expressed and purified from *E. coli* as described previously.[12] Excess FMN (riboflavin 5'-monophosphate sodium salt, Sigma) was added to purified iLOV, and unbound FMN removed by centrifugal filtration before further purification by size exclusion (Sephacryl S-200 HR 16/60, GE Healthcare).

UV-visible absorption and emission spectroscopy

All spectra of FMN and iLOV were acquired in 50 mM Tris-HCl, pH8, 50 mM NaCl. All UV-visible absorption spectra were acquired in a 1 cm path length quartz cuvette using an Agilent Cary 60 UV-Vis Spectrophotometer. All fluorescence measurements were carried out using a FLS920 Edinburgh Instruments Spectrofluorometer. Fluorescence emission spectra were acquired for an excitation wavelength of 450 nm, and fluorescence lifetimes after excitation at 474 nm (from an Edinburgh Instruments EPL470 picosecond pulsed diode laser) and detection at 530 nm using time correlated single photon counting (PCS900 plug-in PC card for fast photon counting). Lifetimes were obtained by tail fit to the data obtained or by a reconvolution fit using a solution of Ludox® as the scatterer, and quality of fit judged by minimisation of reduced chi-squared and residuals squared.

iLOV extinction coefficient.

Absorption spectra were measured using a Shimadzu MultiSpec-1501 diode array spectrophotometer at room temperature. The optical path length was 0.5 cm and protein concentrations were determined by the BCA protein assay (Thermo Fisher Scientific) using Bovine Serum Albumin as standard. Denatured samples were prepared by incubation at 100 °C for 15 min in 10 % (w/v) SDS. The concentration of liberated FMN was calculated from its peak absorption at ~ 450 nm using an extinction coefficient, ε450 = 12.2 mM-1 cm-1.[33] The ε450 for iLOV was then calculated from that of FMN and the ratio of their peak signal intensities.

Fluorescence quantum yield of iLOV

The fluorescence quantum yield, φ_s, of iLOV (sample) was calculated using a comparative method[53] where the integrated fluorescence intensity of iLOV was related to that of FMN (reference, φ_r = 0.25).[33] Measurements were made across a number of reference and sample concentrations within the range 0 – 1.0 absorbance units at the excitation wavelength (450 nm). The integrated fluorescence intensity was then plot for both sample and reference as a function of peak absorbance at each concentration and the φ_s of iLOV was then calculated using:

$$\Phi_s = \Phi_r \left(\frac{m_s}{m_r}\right)\left(\frac{\eta_s^2}{\eta_r^2}\right) \quad (1)$$

where, m_s and m_r at the gradient of the linear fits for sample and reference. Both the sample and reference were in aqueous solution and therefore their respective refractive indices, η, are that of water; the term containing η in equation 1 is therefore equal to 1. Although φ_s for iLOV has been estimated previously,[15] the value of φ_s ~ 0.44 was calculated based on the assumption that ε_{450} for FMN and iLOV are the same. Here, we corrected this to account for the ε_{450} that we have estimated for iLOV: *i.e.*, ε_{450} (FMN) = 12.2 mM^{-1} cm^{-1} and ε_{450} (iLOV) = 17.6 mM^{-1} cm^{-1}.

Two photon cross sections

2P fluorescence measurements we made by focussing the tuneable output of a Spectra-Physics Mai Tai Ti:Sapphire oscillator (100 fs, 80 MHz) onto the sample using an extra long working distance (ELWD), 40× air immersion objective (Nikon plan fluor ELWD: 2.80-3.60mm, 0.6 NA). The fluorescence was detected in epifluorescence mode *via* a longpass dichroic mirror with a cut-on wavelength of 650 nm (Thor Labs, FEL0650). To reduce residual and scattered laser light several shortpass filters were used, with cut-off wavelengths of 700, 800 and 900 nm (Thor Labs, FES0700, FES0800 and FES0900). Fluorescence was collected by a compact CCD spectrometer module (Ocean Optics QE65000) and processed using SpectraSuite®. The laser power was varied using a neutral density filter, and the emission spectra were integrated over the region of maximum emission, ± 2 nm. Two photon cross sections, $\sigma_{2,s}$, for FMN and iLOV (sample) were calculated[42] every 5 nm in the region 730 – 970 nm with reference to concurrent and equivalent measurements with a fluorescent reference that has a known and appropriate $\sigma_{2,r}$ spectrum (fluorescein, Sigma, reference)[43] using:

$$\sigma_{2,s} = \frac{F_{2,s} C_r \phi_r}{F_{2,r} C_s \phi_s} \sigma_{2,r} \quad (2)$$

where: $F_{2,s}$ and $F_{2,r}$ are the integrated fluorescent intensities at each excitation wavelength; C_s (both FMN and iLOV 70 – 80 μM, in 50 mM Tris-HCl, pH8, 50 mM NaCl) and C_r (fluorescein ~ 11 μM, in 100 mM $NaOH_{(aq)}$) are the species concentrations; φ_s (iLOV = 0.3; FMN = 0.25) and φ_r (fluorescein = 0.95) are the fluorescence quantum yields; the sub-script descriptors 's' and 'r' refer to the sample and reference parameters, respectively.

Mammalian cell culture, transfection and expression

iLOV-N1 plasmid[15] and pEGFPN1 empty vector control plasmid (Takara) were amplified by transformation into DH5a competent *E.coli* cells (NEB) and growth in LB media with 25 μg ml^{-1} kanamycin (Sigma). High quality DNA was prepared using a Maxi prep kit (Qiagen). HEK293 cells (ATCC) were grown in DMEM media (Sigma) supplemented with 10% FBS (Sigma), 2 U ml^{-1} Penicillin and 2 mg ml^{-1} streptomycin (Sigma) and 2mM glutamine (ThermoFisher Scientific) at 37 °C in a humidified 5% CO_2 incubator. Prior to transfection the HEK293 cells were trypsinised (ThermoFisher Scientific) and plated on 10 cm^2 Nunc petri dishes (ThermoFisher Scientific) at 70% confluency. Media were removed and replaced with reduced serum Opti-MEM (ThermoFisher Scientific) without antibiotics and plasmid DNAs transfected using Lipofectamine (ThermoFisher Scientific) according to the manufacturer's protocol. The ratio of 24 μg of plasmid to 60 μl of lipofectamine was found to be optimal. Transfected cells were left for 48hrs at 37 °C to allow a high level of protein expression.

Fluorescence microscopy

1P and 2P fluorescence microscopy images of HEK293 cells expressing iLOV were collected on a Leica SP8 Upright Multiphoton microscope using a 40×, 1.10 NA HC PL Apo water-immersion objective and 2x zoom. Images were collected using hybrid detectors with fixed filters (BP624/40, HyD3-mCherry; BP525/50, HyD4-GFP). 2P excitation at 750, 860 and 900 nm was achieved using a Mai Tai MP Ti:Sapphire oscillator (Spectra Physics) attenuated to 3% of maximum power. For the data in Figure 4, this corresponds to laser powers at the sample plane of 18.4 mW (860 nm) and 17.5 mW (900 nm). Multichannel images were collected sequentially. When acquiring 3D optical stacks the multiphoton software was used to determine the optimal number of Z sections. Only the maximum intensity projections of these 3D stacks are shown in the results. 1P excitation (488 nm) was achieved using a diode laser attenuated to 10% of maximum power, which corresponds to a laser power at the sample plane of 17 μW. 1P images were collected in the confocal regime using a pinhole diameter of 1 airy unit.

Conflicts of interest

There are no conflicts to declare.

Acknowledgements

We thank Dr. Sam Hay (Chemistry, Manchester) for support with the fluorescence lifetime measurements and Dr. Patrick Parkinson (Physics, Manchester) for support with the 2P spectroscopy. ARJ thanks The University of Manchester, The Royal Society (RG160676), and FP7 'MAGIC' Innovative Doctoral Programme (606831) for funding. JMC thanks funding support from the UK Biotechnology and Biological Sciences Research Council (BB/M002128/1) and an IBioIC PhD Studentship (AEK). LSN thanks the Leverhulme Trust for postdoctoral funding (MBA) and a research Leadership award (LSN, RL-2012-072).

References

1. J. M. Christie, *Annu. Rev. Plant Biol.*, 2007, **58**, 21-45.
2. J. Herrou and S. Crosson, *Nat Rev Microbiol*, 2011, **9**.
3. T. E. Swartz, S. B. Corchnoy, J. M. Christie, J. W. Lewis, I. Szundi, W. R. Briggs and R. A. Bogomolni, *J. Biol. Chem.*, 2001, **276**, 36493-36500.
4. J. T. M. Kennis, S. Crosson, M. Gauden, I. H. M. van Stokkum, K. Moffat and R. van Grondelle, *Biochemistry*, 2003, **42**, 3385-3392.
5. M. Salomon, J. M. Christie, E. Knieb, U. Lempert and W. R. Briggs, *Biochemistry*, 2000, **39**, 9401-9410.
6. S. M. Harper, L. C. Neil and K. H. Gardner, *Science*, 2003, **301**, 1541-1544.
7. S. T. Glantz, E. J. Carpenter, M. Melkonian, K. H. Gardner, E. S. Boyden, G. K.-S. Wong and B. Y. Chow, *Proc. Natl. Acad. Sci. USA*, 2016, **113**, E1442-E1451.
8. S. Crosson, S. Rajagopal and K. Moffat, *Biochemistry*, 2003, **42**, 2-10.
9. T. Schafmeier and A. C. R. Diernfellner, *FEBS Lett*, 2011, **585**, 1467-1473.
10. J. M. Christie, J. Gawthorne, G. Young, N. J. Fraser and A. J. Roe, *Molecular Plant*, 2012, **5**, 533-544.
11. T. Climent, R. González-Luque, M. Merchán and L. Serrano-Andrés, *J. Phys. Chem. A*, 2006, **110**, 13584-13590.
12. J. M. Christie, K. Hitomi, A. S. Arvai, K. A. Hartfield, M. Mettlen, A. J. Pratt, J. A. Tainer and E. D. Getzoff, *J. Biol. Chem.*, 2012, **287**, 22295-22304.
13. T. Drepper, T. Gensch and M. Pohl, *Photochem. Photobiol. Sci.*, 2013, **12**, 1125-1134.
14. A. M. Buckley, J. Petersen, A. J. Roe, G. R. Douce and J. M. Christie, *Curr. Opin. Chem. Biol.*, 2015, **27**, 39-45.
15. S. Chapman, C. Faulkner, E. Kaiserli, C. Garcia-Mata, E. I. Savenkov, A. G. Roberts, K. J. Oparka and J. M. Christie, *Proc. Natl. Acad. Sci. USA*, 2008, **105**, 20038-20043.
16. X. Shu, V. Lev-Ram, T. J. Deerinck, Y. Qi, E. B. Ramko, M. W. Davidson, Y. Jin, M. H. Ellisman and R. Y. Tsien, *PLOS Biology*, 2011, **9**, e1001041.
17. T. Drepper, T. Eggert, F. Circolone, A. Heck, U. Krausz, J.-K. Guterl, M. Wendorff, A. Losi, W. Gartner and K.-E. Jaeger, *Nat Biotech*, 2007, **25**, 443-445.
18. A. Mukherjee, J. Walker, K. B. Weyant and C. M. Schroeder, *PLoS ONE*, 2013, **8**.
19. A. Mukherjee, K. B. Weyant, J. Walker and C. M. Schroeder, *J. Biol. Eng.*, 2012, **6**, 20.
20. J. Torra, A. Burgos-Caminal, S. Endres, M. Wingen, T. Drepper, T. Gensch, R. Ruiz-Gonzalez and S. Nonell, *Photochem. Photobiol. Sci.*, 2015, **14**, 280-287.
21. A. Mukherjee, K. B. Weyant, U. Agrawal, J. Walker, I. K. O. Cann and C. M. Schroeder, *ACS Synth. Biol.*, 2015, **4**, 371-377.

22. J. Seago, N. Juleff, K. Moffat, S. Berryman, J. M. Christie, B. Charleston and T. Jackson, *J. Gen. Virol.*, 2013, **94**, 1517-1527.
23. T. Drepper, R. Huber, A. Heck, F. Circolone, A.-K. Hillmer, J. Büchs and K.-E. Jaeger, *Appl. Environ. Microbiol.*, 2010, **76**, 5990-5994.
24. K. S. Conrad, C. C. Manahan and B. R. Crane, *Nat Chem Biol*, 2014, **10**, 801-809.
25. C. Xu, W. Zipfel, J. B. Shear, R. M. Williams and W. W. Webb, *Proc. Natl. Acad. Sci. USA*, 1996, **93**, 10763-10768.
26. G. A. Blab, P. H. M. Lommerse, L. Cognet, G. S. Harms and T. Schmidt, *Chem. Phys. Lett.*, 2001, **350**, 71-77.
27. N. H. List, F. M. Pimenta, L. Holmegaard, R. L. Jensen, M. Etzerodt, T. Schwabe, J. Kongsted, P. R. Ogilby and O. Christiansen, *Phys. Chem. Chem. Phys.*, 2014, **16**, 9950-9959.
28. W. Denk, J. Strickler and W. Webb, *Science*, 1990, **248**, 73-76.
29. E. Brown, T. McKee, E. diTomaso, A. Pluen, B. Seed, Y. Boucher and R. K. Jain, *Nat Med*, 2003, **9**, 796.
30. K. König, *J Mic*, 2000, **200**, 83-104.
31. R. Prakash, O. Yizhar, B. Grewe, C. Ramakrishnan, N. Wang, I. Goshen, A. M. Packer, D. S. Peterka, R. Yuste, M. J. Schnitzer and K. Deisseroth, *Nat Meth*, 2012, **9**, 1171-1179.
32. B. Klaumünzer, D. Kröner and P. Saalfrank, *J. Phys. Chem. B*, 2010, **114**, 10826-10834.
33. M. Wingen, J. Potzkei, S. Endres, G. Casini, C. Rupprecht, C. Fahlke, U. Krauss, K. E. Jaeger, T. Drepper and T. Gensch, *Photochem. Photobiol. Sci.*, 2014, **13**, 875-883.
34. M. D. Davari, B. Kopka, M. Wingen, M. Bocola, T. Drepper, K. E. Jaeger, U. Schwaneberg and U. Krauss, *J. Phys. Chem. B*, 2016, **120**, 3344-3352.
35. B. Bajar, E. Wang, S. Zhang, M. Lin and J. Chu, *Sensors*, 2016, **16**, 1488.
36. J. Potzkei, M. Kunze, T. Drepper, T. Gensch, K.-E. Jaeger and J. Büchs, *BMC Biol.*, 2012, **10**, 28.
37. H. Wallrabe and A. Periasamy, *Curr. Opin. Biotechnol.*, 2005, **16**, 19-27.
38. W. M. McClain, *Acc. Chem. Res.*, 1974, **7**, 129-135.
39. P. R. Callis, *Annu. Rev. Phys. Chem.*, 1997, **48**, 271-297.
40. D. J. Bradley, M. H. R. Hutchinson, H. Koetser, T. Morrow, G. H. C. New and M. S. Petty, *Proc. R. Soc. A.*, 1972, **328**, 97-121.
41. J. R. Lakowicz, I. Gryczynski, V. Bogdanov and J. Kusba, *J. Phys. Chem.*, 1994, **98**, 334-342.
42. N. S. Makarov, M. Drobizhev and A. Rebane, *Opt. Express*, 2008, **16**, 4029-4047.
43. C. Xu and W. W. Webb, *J. Opt. Soc. Am. B*, 1996, **13**, 481-491.
44. H. Hosoi, S. Yamaguchi, H. Mizuno, A. Miyawaki and T. Tahara, *J. Phys. Chem. B*, 2008, **112**, 2761-2763.
45. M. Drobizhev, S. Tillo, N. S. Makarov, T. E. Hughes and A. Rebane, *J. Phys. Chem. B*, 2009, **113**, 855-859.
46. E. Kamarchik and A. I. Krylov, *J. Phys. Chem. Lett.*, 2011, **2**, 488-492.
47. M. Drobizhev, N. S. Makarov, S. E. Tillo, T. E. Hughes and A. Rebane, *Nat. Meth.*, 2011, **8**, 393.
48. M. Drobizhev, S. Tillo, N. S. Makarov, T. E. Hughes and A. Rebane, *J. Phys. Chem. B*, 2009, **113**, 12860-12864.
49. M. Drobizhev, N. S. Makarov, S. E. Tillo, T. E. Hughes and A. Rebane, *J. Phys. Chem. B*, 2012, **116**, 1736-1744.
50. I. Gregor, M. Spiecker, R. Petrovsky, J. Großhans, R. Ros and J. Enderlein, *Nat. Meth.*, 2017, **14**, 1087.
51. K. Deisseroth, *Nat. Methods*, 2011, **8**, 26-29.
52. H. Mikami, L. Gao and K. Goda, *Journal*, 2016, **5**, 497.
53. A. T. R. Williams, S. A. Winfield and J. N. Miller, *Analyst*, 1983, **108**, 1067-1071.